

See discussions, stats, and author profiles for this publication at: <https://www.researchgate.net/publication/40448853>

Crystal Structure of the Light-Driven Chloride Pump Halorhodopsin from *Natronomonas pharaonis*

ARTICLE in JOURNAL OF MOLECULAR BIOLOGY · DECEMBER 2009

Impact Factor: 4.33 · DOI: 10.1016/j.jmb.2009.11.061 · Source: PubMed

CITATIONS

54

READS

48

6 AUTHORS, INCLUDING:



Tsutomu Kouyama

Nagoya University

69 PUBLICATIONS 2,047 CITATIONS

[SEE PROFILE](#)



Kunio Ihara

Nagoya University

59 PUBLICATIONS 1,028 CITATIONS

[SEE PROFILE](#)



Crystal Structure of the Light-Driven Chloride Pump Halorhodopsin from *Natronomonas pharaonis*

Tsutomu Kouyama^{1*}, Soun Kanada¹, Yuu Takeguchi¹,
Akihiro Narusawa¹, Midori Murakami¹ and Kunio Ihara²

¹Department of Physics,
Graduate School of Science,
Nagoya University, Chikusa-ku,
Nagoya 464-8602, Japan

²Center for Gene Research,
Nagoya University, Chikusa-ku,
Nagoya 464-8602, Japan

Received 30 September 2009;

received in revised form

21 November 2009;

accepted 24 November 2009

Available online

1 December 2009

The light-driven chloride pump halorhodopsin from *Natronomonas pharaonis* (phR) crystallised into the monoclinic space group C2, with a phR trimer per the asymmetric unit. Diffraction data at 2.0-Å resolution showed that the carotenoid bacterioruberin binds to crevices between adjacent protein subunits in the trimeric assembly. Besides seven transmembrane helices (A to G) that characterise archaeal rhodopsins, the phR protomer possesses an amphipathic α -helix (A') at the N-terminus. This helix, together with a long loop between helices B and C, forms a hydrophobic cap that covers the extracellular surface and prevents a rapid ion exchange between the active centre and the extracellular medium. The retinal bound to Lys256 in helix G takes on an all-trans configuration with the Schiff base being hydrogen-bonded to a water molecule. The Schiff base also interacts with Asp252 and a chloride ion, the latter being fixed by two polar groups (Thr126 and Ser130) in helix C. In the anion uptake pathway, four ionisable residues (Arg123, Glu234, Arg176 and His100) and seven water molecules are aligned to form a long hydrogen-bonding network. Conversely, the cytoplasmic half is filled mostly by hydrophobic residues, forming a large energetic barrier against the transport of anion. The height of this barrier would be lowered substantially if the cytoplasmic half functions as a proton/HCl antiporter. Interestingly, there is a long cavity extending from the main-chain carbonyl of Lys256 to Thr71 in helix B. This cavity, which is commonly seen in halobacterial light-driven proton pumps, is one possible pathway that is utilised for a water-mediated proton transfer from the cytoplasmic medium to the anion, which is relocated to the cytoplasmic channel during the photocycle.

© 2009 Elsevier Ltd. All rights reserved.

Edited by J. Bowie

Keywords: chloride ion pump; halorhodopsin; retinal; bacterioruberin; proton pump

Introduction

Halorhodopsin (HR), a member of archaeal rhodopsins, occurs ubiquitously in halobacteria. It contains retinal as a chromophore and uses light energy to import the chloride ion into the cell against the membrane potential.^{1–3} To date, HR homologs from *Halobacterium salinarum* and *Natronomonas pharaonis* have been extensively investigated.^{4–14} In

H. salinarum, which possesses the light-driven proton pump bacteriorhodopsin (BR) as a principal component in the bioenergetic system, HR is believed to play a role in maintaining osmotic balance during cell growth.¹⁵ In *N. pharaonis*, which grows optimally at pH 9.0–10.0, BR is lacking and instead HR participates in the generation of metabolic energy.^{16–18} The HR homologs from *H. salinarum* and *N. pharaonis* are hereafter referred to as *salinarum* HR (shR) and *pharaonis* HR (phR), respectively, because they differ in many aspects. First, the polypeptide of phR is 17 residues longer than that of shR mainly because of the insertion of 5 residues in the N-terminal region and 10 residues in the BC loops^{16,19,20} (Fig. 1). Reflecting the low sequence identity (55%) between shR and phR, there are profound differences in their ion specificity,

*Corresponding author. E-mail address:
kouyama@bio.phys.nagoya-u.ac.jp.

Abbreviations used: pHr, *Natronomonas pharaonis* halorhodopsin; shR, *Halobacterium salinarum* halorhodopsin; BR, bacteriorhodopsin; aR2, archaerhodopsin-2.

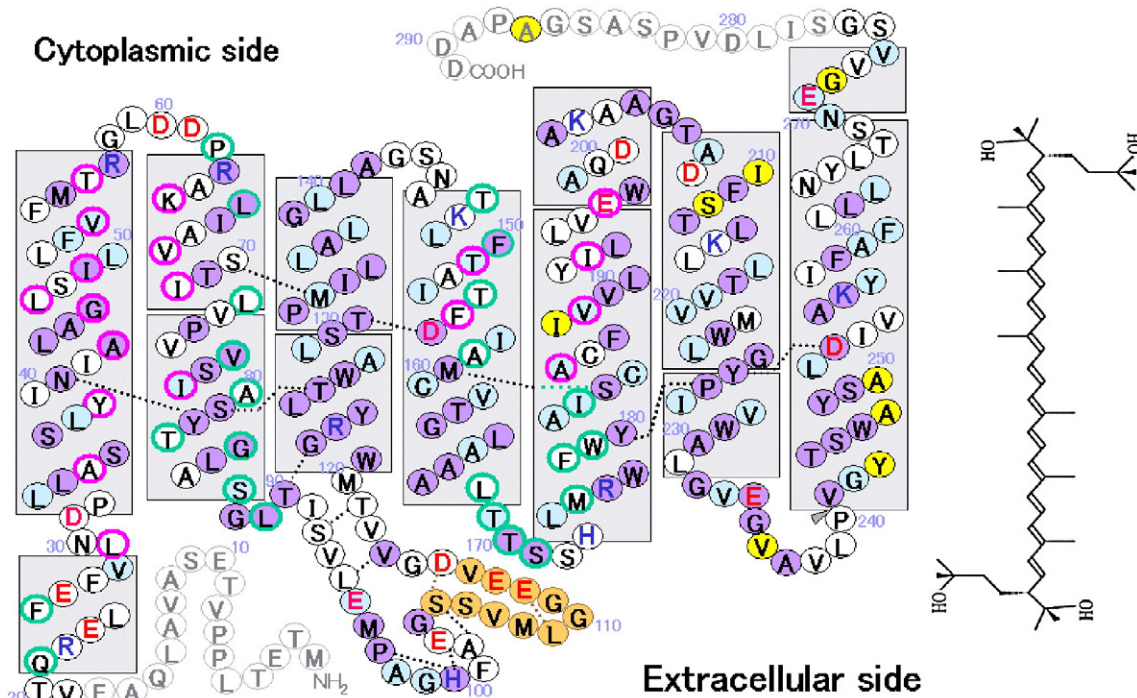


Fig. 1. (a) Schematic diagram of the topology of phR showing helices as rectangles. Residues contacting bacterioruberin and residues participating in intra-trimer protein–protein interactions are framed with magenta and green circles, respectively. Violet and light blue circles represent residues conserved between phR and shR, whereas orange circles show inserted residues found only in phR. (Residues conserved among all known HR homologs are marked with violet circles.) Yellow circles denote residues that are not conserved between the two type strains of *N. pharaonis* (DSM 2160^T and DSM 3395^T). Residues excluded from the structural model of phR are shown by grey letters. (b) Chemical structure of bacterioruberin.

spectroscopic property and kinetic behaviour. For example, the removal of Cl⁻ from phR causes a 20-nm red shift of the visible absorption band,²¹ whereas shR shows a 10-nm blue shift on the removal of Cl⁻.²² The dissociation constants of chloride for phR and shR were reported to be ~1 and ~10 mM, respectively.^{21,23,24} Whereas at least four intermediates (K, L1, L2 and O) have been identified in the anion-transporting photocycle of phR,²⁵ the O intermediate is undetectable in the photocycle of the *trans* form of shR for kinetic reasons.²⁶ It is important to accumulate structural information on these proteins to clarify the origins of these differences and better understand the transport mechanism of anion.

The first structural information about HR was provided by cryo-electron microscopy of tetragonal two-dimensional crystals that formed spontaneously when shR was overproduced in the strain L33 (*bop*⁻, *rub*⁻) of *H. salinarum*.²⁷ Although this crystal was a physiologically irrelevant artifact produced under the overexpression condition, the structural data of up to 5-Å resolution revealed the overall architecture of HR. A more detailed structural model of shR was built by Kolbe *et al.*, who prepared hexagonal P6₃22 crystals by the lipidic cubic phase method.²⁸ More recently, Gmelin *et al.* prepared another crystal form (space group R32) of an shR mutant (Thr203 → Val) to determine the

structure of the photoreaction L1 intermediate.²⁹ According to their result, a small movement of the chloride ion (0.3 Å away from the Schiff base) was induced upon formation of the L1 state. However, it remains unclear how much the mutation affects light-induced movement of a chloride ion. In fact, the importance of Thr203 for binding of Cl⁻ to the cytoplasmic channel in shR was previously demonstrated.³⁰ Unfortunately, nobody has succeeded in getting structural information about the photoreaction intermediates of wild-type shR. This difficulty might come from the coexistence of two retinal isomers in the light-adapted state of shR.³¹ By contrast, it was previously reported that the light-adapted state of phR contains the retinal isomer with an all-*trans* configuration as the major component and that the 13-*cis* isomer does not show photoactivity.³² Against this background, the objective is to prepare a three-dimensional crystal of phR suitable for acquiring structural information about how the chloride ion is transported.

In a previous study, an HR (phR)-overproducing strain (designated as KM-1) was generated by UV mutagenesis from the type strain of *N. pharaonis*, JCM 8858T (DSM 2160^T).¹⁶ Genetic analysis showed that the overexpression of phR was caused by a point mutation in the BR activator homolog of *N. pharaonis*, whereas the amino acid sequence of phR was unaltered. [Note that phR in the type strain

DSM 2160^T differs slightly from the HR expressed in SP1 (DSM 3395^T), another type strain, which has been investigated in other laboratories (marked with yellow circles in Fig. 1).] The expression level of *phR* in the strain KM-1 is ~50 times higher than that in the wild-type strain, and, unlike an overexpression system of *shR*, the overproduction of *phR* does not deteriorate the cell activity. The *phR*-enriched membrane isolated from the cell membranes exhibits claret owing to the second chromophore bacterioruberin. From the observation that the absorption band of bacterioruberin was perturbed upon the chloride binding, it was suggested that bacterioruberin interacts strongly with *phR*.¹⁶

In this study, the trimeric *phR*-bacterioruberin complex was crystallised into a monoclinic crystal belonging to space group C2. Diffraction data at 2.0-Å resolution showed that the quaternary structure of *phR* is very similar to those observed in the hexagonal crystals of archaerhodopsin-2 (ar2),³³ a light-driven proton pump found in the claret membrane of *Halorubrum* sp. aus-2. Structural comparison with other archaeal rhodopsins revealed a unique structural motif possessed only by *phR*. First, the N-terminal polypeptide is folded into a helical segment. This helix, together with the extracellular BC loop, forms a large hydrophobic cap covering most areas of the extracellular surface of the protein. A substantial difference between *phR* and *shR* is also seen in the structure of the primary binding site of the chloride ion. The physiological meaning of these differences will be discussed.

Results

Crystals prepared by the membrane fusion method

When cells of the *N. pharaonis* strain KM-1 were washed with distilled water, a *phR*-enriched fraction was isolated as claret vesicles with a diameter of 50 to ~400 nm. The absorption spectrum of a suspension of the claret vesicles in 0.1 M NaCl was characterised by vibronic bands of bacterioruberin with peaks at 475, 504 and 540 nm and a broad band of retinal with a peak at 578 nm. The latter band shifted to 600 nm when the salt concentration was lowered below 1 mM.¹⁶ When the claret vesicles were partially delipidated with 0.5% Tween-20, a considerable fraction of bacterioruberin was removed. However, bacterioruberin remained a predominant pigment in the vesicle membranes that were repeatedly washed with Tween-20. Together with the previous observation that the chloride binding to *phR* was accompanied by a noticeable sharpening of the vibronic band of bacterioruberin,¹⁶ this observation suggests that bacterioruberin is bound strongly to *phR*.

With the aim of acquiring structural information about the binding mode of bacterioruberin to *phR*, we adopted the same crystallisation method as

previously used for the structural determination of the trimeric ar2-bacterioruberin complex. First, Tween-20-treated claret membranes were dissolved in 0.5% nonylglucoside, 0.16 M NaCl, 1 M ammonium sulfate and 0.04 M Tris buffer, pH 8.0. After the mixture solution was centrifuged at 10,000 rpm to remove a large fraction of other protein components, a drop of the supernatant, in which *phR* accounted for >70% of the total protein, was placed on a lower glass in a crystallisation kit and equilibrated with a reservoir solution containing 2.4–2.9 M ammonium sulfate. Incubation at 288 K for several weeks yielded monoclinic crystals of *phR*. Large crystals grew preferentially within a claret protein-rich phase floating near the top of the crystallisation drop (Fig. 2a), whereas much smaller crystals grew on the surface of the lower glass in the crystallisation kit (Fig. 2c). The phase separation preceding the crystal growth is commonly observed when archaeal rhodopsins are crystallised by the membrane fusion method.^{33,34}

Optical properties of the monoclinic crystal

Thin crystals adhered to the lower glass were used for the investigation of the crystal properties. A small fraction of such crystals looked like purple parallelogram plates with an apex angle of ~87° (Fig. 2b). When the crystal was viewed from the top of the crystallisation solution, it exhibited no birefringence. [It was subsequently shown that this outlook of crystal would be reproducible if a principal crystal axis (the *b*-axis) is parallel with the normal to the glass plate.]

Conversely, most crystals looked like rectangular plates and exhibited strong birefringence (Fig. 2c). When these crystals were investigated under a polarising microscope, their colour varied with the direction of the polarisation plane. Figure 2d shows their absorption spectra recorded with polarised light. It is clear that the crystal contains two types of chromophores (i.e., retinal and bacterioruberin) whose absorption dipole moments are differently oriented. The colour change induced by rotating the polarisation plane became undetectable when the lower glass was tilted by ~45° around the long axis of one of the crystals shown in Fig. 2c. Conversely, this colour change became more significant when the lower glass was tilted in the reverse direction (i.e., the crystal exhibited purple when the polarisation plane was parallel with the long axis of the crystal, whereas it turned orange when the polarisation plane was rotated by 90°). These observations provide the following information about the chromophore orientations in the crystal: (1) the absorption dipole moment of bacterioruberin orients nearly parallel with a direction (assigned to the *b*-axis) that is perpendicular to the long axis of the crystal; (2) the absorption dipole moment of retinal orients nearly perpendicular to the *b*-axis; and (3) the crystal grew faster in a direction perpendicular to the *b*-axis. For the crystals shown in Fig. 2c, the *b*-axis is tilted 35°–40° from the normal of the lower glass. (The tilt

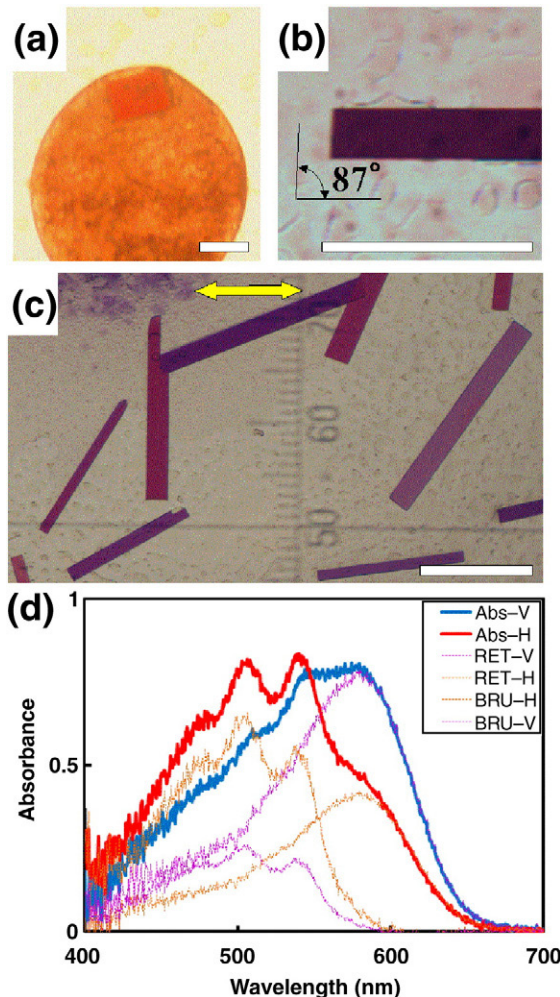


Fig. 2. (a) A phR crystal grown within a claret protein-rich phase floating near the top of the crystallisation solution. The crystal was visualised by utilising its birefringence; that is, the amount of light passing through the surrounding medium was attenuated by adjusting the orientations of the polariser and analyser in a polarising microscope. Scale bar: 0.1 mm. (b, c) phR crystals adhered to the lower glass in a crystallisation kit. The arrow in (c) indicates the direction of the polarisation plane of the measuring light. (d) Absorption spectra of one of the crystals shown in (c) were measured with polarised light. Blue and red lines represent the spectra recorded when the polarisation plane was parallel and when it was perpendicular to the long axis of the crystal, respectively. Thin purple and orange lines denote the absorption components of retinal and bacterioruberin, respectively.

angle is estimated roughly because the refractive index of the crystal is unknown.)

When the spectra shown in Fig. 2d are analysed on the assumption that there is no strong excitation coupling between adjacent chromophores, it is suggested that the retinal chromophore in the crystal has an absorption peak at 578 nm, whereas the vibronic band of bacterioruberin has peaks at 540, 503 and 475 nm. When the crystal orientation is taken into account, the decomposed absorption spectra suggested that the molar ratio of bacterior-

uberin to retinal in the crystal is close to the level expected if one molecule of bacterioruberin is bound to each protein.

Crystal packing

Figure 3 shows the crystal packing in the monoclinic C2 crystal of phR. Three proteins are contained in the asymmetric unit; that is, the unit cell contains four trimers related by the crystallographic 2-fold axes and 2-fold screw axes. The side view of the unit cell shows that the crystal is made up of stacked membranes, in each of which trimers are arranged on striped lines aligned along the shorter diagonal line drawn between the *a*-axis and the *c*-axis. There is no significant structural difference among the three subunits contained in the asymmetric unit (Fig. 3d). The individual protein is composed of seven transmembrane α -helices (A to G), an amphipathic α -helix (A') in the N-terminal region, a short 3_{10} -helix in the C-terminal region and a long extracellular loop formed between helices B and C.

There are four types of inter-trimer interactions that contribute to the crystal packing. One of them is seen around a crystallographic 2-fold axis, where subunit A in one trimer contacts subunit $A_{\text{sym}-1}$ in the adjacent trimer. In this contact region, hydrophobic residues in the cytoplasmic halves of helices F and G mediate direct protein–protein interactions (Fig. 3c). In addition, Tyr243 at the extracellular end of helix G interacts with its counterpart in the adjacent trimer. These inter-trimer interactions define the orientation of each trimer, whose local 3-fold axis is tilted by $\sim 5^\circ$ from the crystal *b*-axis. Reflecting strong interactions between subunits A and $A_{\text{sym}-1}$ (Fig. 3c), the motional freedom of subunit A is suppressed compared with the other subunits (Fig. 3f).

The second type of inter-trimer contact is seen around another 2-fold axis where an open space between the adjacent trimers is filled by lipid molecules. Conversely, the crystal outlooks shown in Fig. 2b are explained by supposing that the crystal growth rate is faster in a direction parallel with the shorter diagonal line between the *a*-axis and the *b*-axis. This implies that the lipid-mediated inter-trimer interactions also play an important role in the crystal packing. However, because residues in helices existing near this 2-fold axis (i.e., helices E and F of subunit B and helices A and G of subunit C) are characterised by large *B*-factors (Fig. 3f), it might be argued that the lipid-mediated inter-trimer interactions are ineffective in fixing the protein positions.

The third type of inter-trimer contact is seen around a 2-fold screw axis where residues (Ser269, Glu271 and Gly272) at 3_{10} -helix G' of subunit B are hydrogen-bonded to Glu26 and Gln30 in helix A' of subunit $B_{\text{sym}-2}$ in the adjunct trimer (Fig. 3e). This contact is further strengthened by a hydrogen bond between Arg57 in helix A of subunit B and the main-chain CO of Gly111 in the BC loop of subunit $B_{\text{sym}-2}$. Because of these interactions, residues in helix A'

Table 1. Data collection and final refinement statistics

Data collection	
Resolution (Å)	60.0–2.0
Space group	C2
Unit cell parameters	
<i>a/b/c</i> (Unit cell Å)	151.83/99.77/99.27
$\alpha/\beta/\gamma$ (°)	90.0/127.67/90.0
Data completion (outer shell) (%)	99.5 (100.0)
Number of unique reflections	78,620 (11,508)
Multiplicity	2.7 (2.7)
$R_{\text{sym}}^{\text{a}}$ (outer shell) (%)	0.072 (0.556)
I/σ (outer shell)	9.9 (2.0)
Refinement	
Resolution limit (Å)	15.0–2.0
Protein residues	259
Number of water molecules	113
Number of chloride ions	6
Number of bacterioruberin	3
Number of lipid molecules	3
$R_{\text{cryst}}^{\text{b}}$ (%)	0.253
R_{free} (%) ^b	0.276
RMSD of bond length (Å)	0.0068
RMSD of bond angle (°)	1.147

^a $R_{\text{sym}} = \sum_{hkl} \sum_i |I_i - \langle I \rangle| / \sum_{hkl} \sum_i I_i$, where I_i is the intensity of an individual reflection and $\langle I \rangle$ is the mean intensity obtained from multiple observations of symmetry-related reflections.

^b $R_{\text{cryst}} = \sum_{hkl} (F_o - |F_c|) / \sum_{hkl} |F_o|$ (5% randomly omitted reflections were used for R_{free}).

and the BC loop of subunit B are characterised by low *B*-factors (Fig. 3f).

A different inter-trimer contact is seen in another 2-fold screw axis; that is, Glu103 in the BC loop of subunit C interacts with Lys202 in the EF loop of subunit C_{sym-3} in the adjunct trimer. However, as judged from the large *B*-factors of these residues, it is suggested that this inter-trimer contact scarcely contributes to the crystal packing. [Since subunit C is not tightly fixed in the unit cell, its refinement is worse than those of subunits A and B. Although the motional freedom of subunit C is considered a demerit from a viewpoint of structural refinement (Table 1), this property may become useful for investigation of light-induced structural changes that would be influenced by crystal lattice force.³⁶]

Trimeric phR–bacterioruberin complex

Figure 4 shows the trimeric phR–bacterioruberin complex found in the asymmetric unit. The second chromophore bacterioruberin binds to crevices between adjacent protomers in the trimeric structure of phR. One terminal end of bacterioruberin is fixed between helices A and B of one protomer and helices D and E of the adjacent protomer. In this inter-subunit crevice, the terminal polar groups of bacterioruberin are hydrogen-bonded to Thr56 OH in one subunit and the side chain of Glu197 in the adjacent subunit. Interestingly, this terminal end also interacts with a chloride ion positioned between Asn147 (and Lys148) of one protomer and Lys65 of the adjacent protomer. The other terminal end is exposed to the extracellular medium and interacts weakly with the polar residues of the protein and an unidentified lipid. In the extracellular part of trimer,

where the inter-protein crevice becomes shallower, bacterioruberin interacts preferentially with the residues from helix A of one protomer.

Besides bacterioruberin-mediated interactions, the trimeric structure is strengthened by direct protein–protein interactions. For example, (1) the side chain of Gln21 in helix A' is hydrogen-bonded to the main chain (Leu168, Thr171 and Ser172) of the DE loop of the adjacent subunit; (2) Ser171 OH in this loop is hydrogen-bonded to the main chain of the BC loop in the other partner; (3) in the cytoplasmic side, Thr147 OH of helix D is hydrogen-bonded to the main chain of the AB loop (Pro62) of the adjacent subunit; and (4) hydrophobic residues from helix D interact tightly with those from helix B of the adjacent protomer. Furthermore, the chloride binding to the inter-protomer crevice also contributes to the stabilisation of the trimeric structure (Fig. 4f). These observations suggest that the trimeric phR–bacterioruberin complex found in the C2 crystal is close to the quaternary structure that phR forms under the physiological conditions.³⁷

The central part of the trimer is filled with lipid molecules. The electron density map suggested that the extracellular half of this region contains three phospholipids. With respect to lipids existing in the cytoplasmic half of this region, the electron density is not clear enough to refine their structures. We cannot exclude the possibility that this space is filled with a special lipid (e.g., cardiolipin) that destroys the local 3-fold symmetry. The apparent disorder of lipids in this region has been observed in the trimeric structures of BR and aR2 in their three-dimensional crystals prepared by the membrane fusion method.^{33,36}

Structure of individual protomers

The retinal chromophore is bound to the ε-amino group of Lys256 via a protonated Schiff base (Fig. 5a). The retinal polyene chain is surrounded by several aromatic residues (Trp127, Tyr180, Phe187, Trp222, Tyr225 and Trp229). The Schiff base NH directs toward the extracellular side so that it is hydrogen-bonded to one of three water molecules (Wat502 to Wat504) that make a special cluster structure in the active centre. The Schiff base also interacts with Asp252 O^{δ1} and a chloride ion, the latter being fixed by two polar groups (Thr126 OH and Ser130 OH) in helix C (Fig. 5b). Wat502 is the unique water molecule hydrogen-bonded to the chloride ion. Wat503 is positioned between Asp252 O^{δ2} and the side chain of Arg123, which is connected to a long hydrogen-bonding network extending to the extracellular surface. Wat504, another water molecule, interacts with Ser81 OH, which is connected to a hydrogen-bonding network extending to

At the extracellular side of Arg123, there is a large cavity filled with a cluster of six water molecules (Wat505 to Wat510). This cavity is terminated by the side chain of Glu234, which in turn is connected to a long hydrogen-bonding network extending to

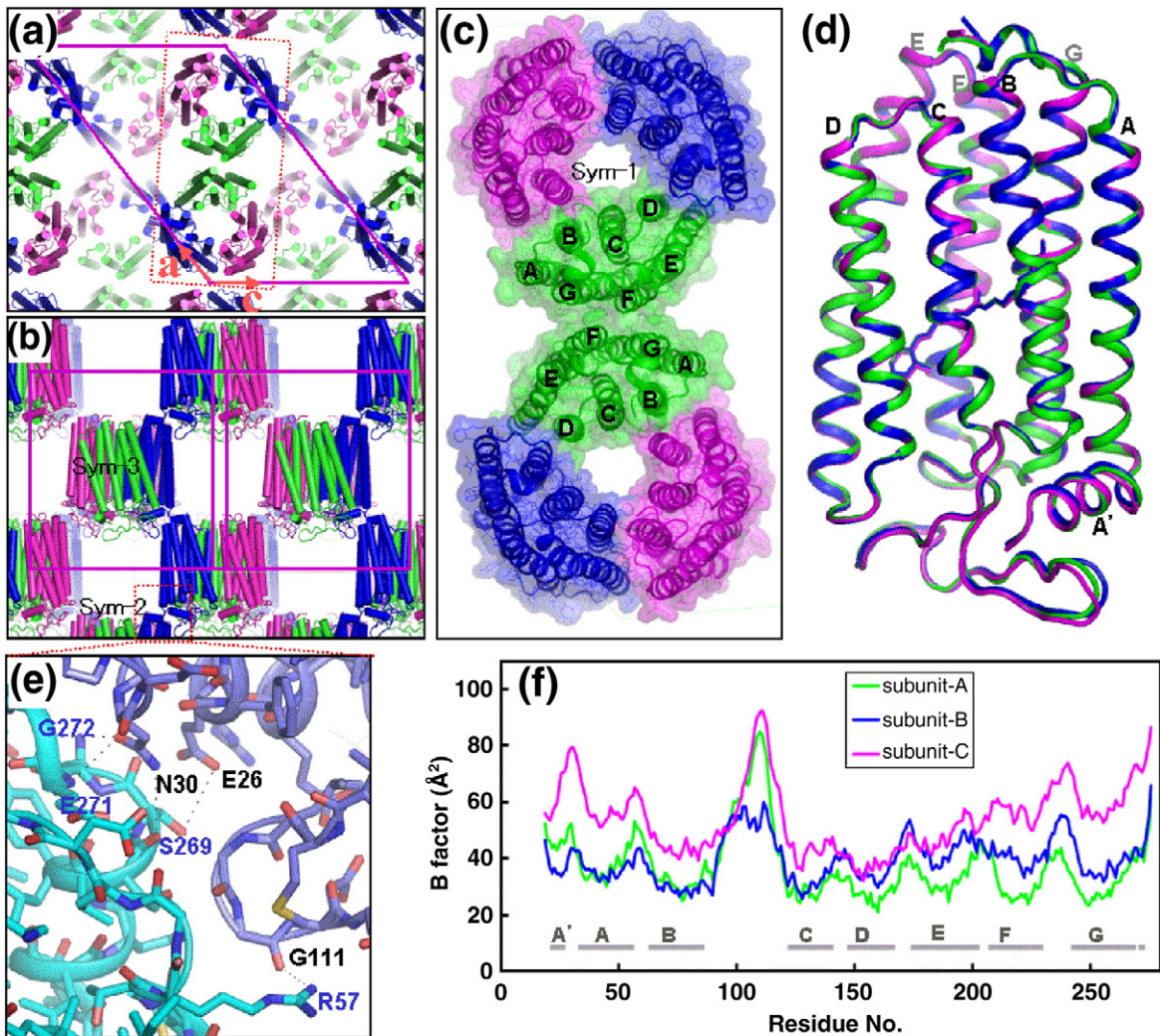


Fig. 3. (a, b) Crystal packing viewed along the *b*-axis (a) and *c*-axis* (b). Three proteins (subunits A, B and C) contained in the asymmetric unit are depicted in green, blue and magenta, respectively. The helices are shown in a cylindrical representation. (c) A pair of trimers positioned around a crystallographic 2-fold axis is viewed along the *b*-axis. The helices in subunits A, B and C are shown in ribbon representation and colour-coded as in (b). The surface of each protein is shown with faint colours. (d) Subunits A (green), B (blue) and C (magenta) are superimposed on one another. (e) Inter-trimer protein–protein interactions around a 2-fold screw axis. O and N atoms are depicted in red and blue, respectively; C atoms are in cyan (subunit B) or violet (subunit B_{sym-2}). (f) B-factors of alpha carbon in subunits A (green), B (blue) and C (magenta) are plotted against the residue number. The images were created with PyMOL.³⁵

His173 at the extracellular surface. This network is constituted by Arg176 in helix F, His100 in the BC loop and two water molecules (Wat511 and Wat512) (Fig. 5c). The four ionisable residues (Arg123, Arg176, Glu234 and His100) aligned between the chloride binding site and the extracellular surface are completely conserved among all HR homologs so far known.³⁸ Thus, it is likely that the hydrogen-bonding network constituted by these residues functions as the major pathway for anion uptake from the extracellular medium.

At the cytoplasmic side of the retinal Schiff base, one water molecule (Wat501) interacts with the indole NH of Trp222, Thr218 OH and the main-chain CO of Ala255 (Fig. 5d). Besides this water molecule, no water molecule with full occupancy exists in the cytoplasmic half of *phR* (Fig. 5e).

Although a large micro-cavity is created between Lys256 CO and Thr71 OH, the occupancy of water in this cavity is low. Other cavities in the cytoplasmic half of *phR* are surrounded by hydrophobic residues, forming a large energetic barrier against the transport of a negatively charged ion.

Helix A' in the N-terminal region possesses three ionisable residues (Arg22, Glu23 and Glu26) that are exposed to the extracellular medium. Conversely, the other face of helix A' possesses hydrophobic residues (Val19, Leu24, Phe25, Phe27 and Val28) (Fig. 5f). These residues interact with hydrophobic residues (Ile91, Val93, Val107, Leu109, Val114 and Val118) in the BC loop. The structure of this loop is not rigid because of a high density of negatively charged residues (Glu95, Glu103, Glu112, Glu113

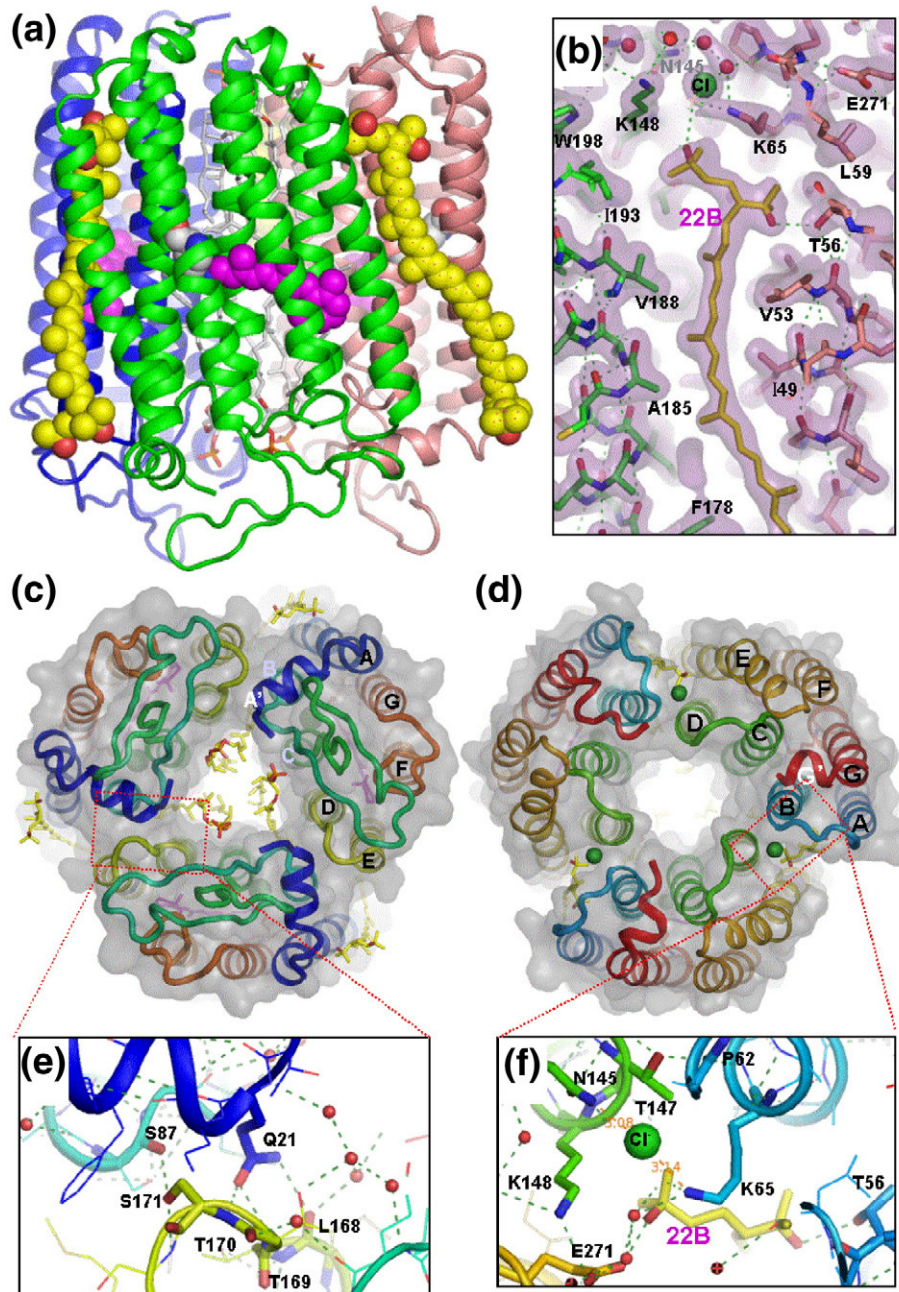


Fig. 4. Architecture of the trimeric phR–bacterioruberin complex. (a) Side view of a phR trimer. Helices are shown in ribbon representation. Retinal (magenta) is bound to Lys256 via a protonated Schiff base, and bacterioruberin (yellow) is bound to a crevice between adjacent subunits. (b) $2F_o - F_c$ maps around bacterioruberin, contoured at 1σ and overlaid on the structural model. (c, d) The trimer is viewed from the extracellular (c) and cytoplasmatic (d) sides. Each polypeptide chain is colour-coded from blue (N-terminus) to red (C-terminus). The surface of protein is shown in grey. (e, f) Intratrimer protein–protein interactions at the extracellular (e) and cytoplasmic (f) surfaces. O and N atoms are shown in red and blue, respectively; C atoms are coloured as in (c) and (d). Red spheres represent water molecules. The green sphere in (f) is a chloride ion.

and Asp115). Nonetheless, hydrophobic residues in the BC loop (including Leu94 and Val117) interact tightly with hydrophobic residues from helix A (Leu34 and Leu38), helix B (Leu85), helix D (Leu174), helix F (Val233) and helix G (Val241). Together with the hydrophobic residues in helix A', they form a hydrophobic cap that covers the extracellular surface of the protein. This hydrophobic cap seems to prevent a rapid exchange of

charged ions between the active centre and the extracellular medium.

The C-terminal polypeptide is folded into a short 3_{10} -helix. Residues from this helix and the AB loop together cover the inter-helical space among helices A, B, C and G (Fig. 4d). Conversely, the cytoplasmic part of helix E is largely bent so that it covers the inter-helical space among helices D, E and F. Together with the CD loop, residues from this loop

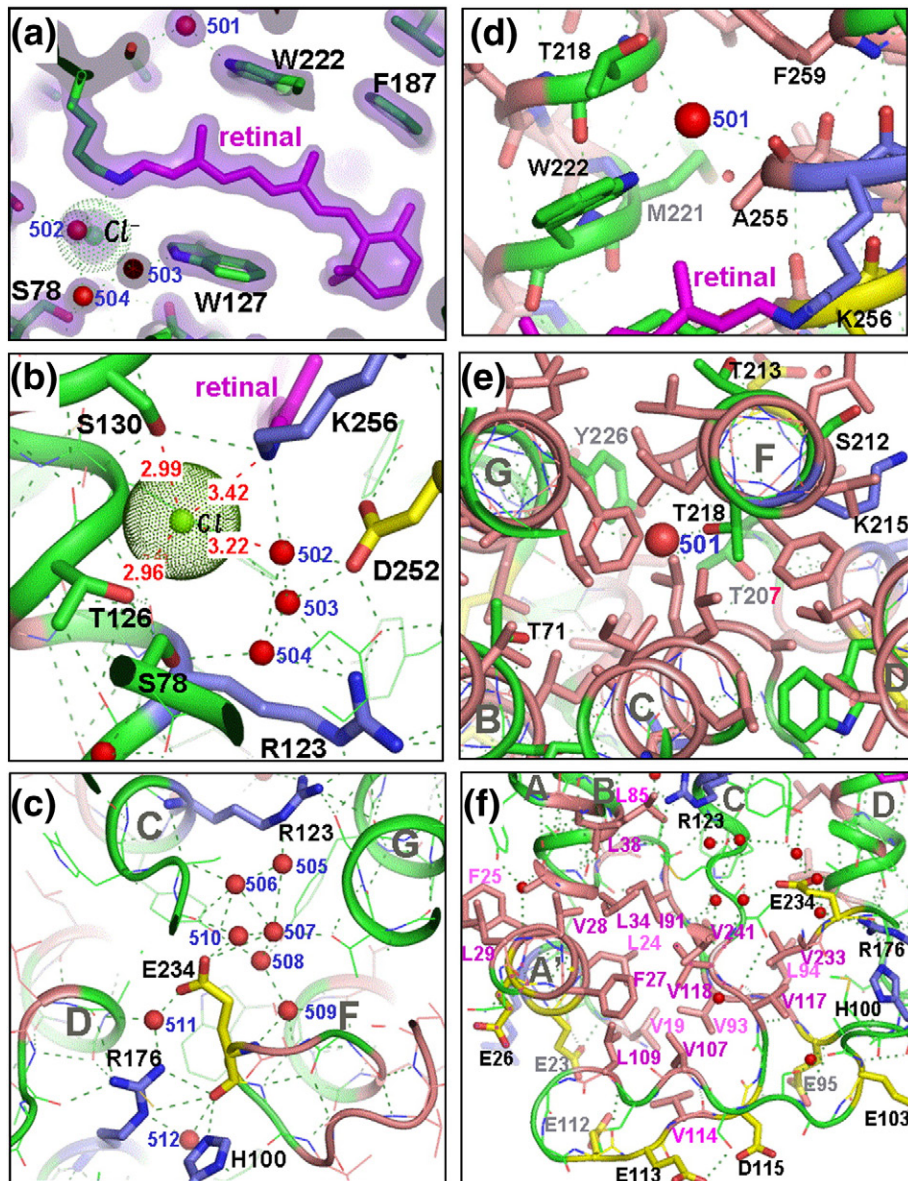


Fig. 5. Structure of pHr (subunit A). (a) 2F_o - F_c map around retinal, contoured at 2σ and overlaid on the structural model. (b) The primary binding site of a chloride ion (yellow-green sphere). Red numerals represent distances (expressed in angstrom) from the chloride ion to surrounding atoms (the retinal Schiff base, Thr126 OH, Ser130 OH and Wat502). (c) A cluster of water molecules (red spheres) in the chloride uptake pathway. (d) A water molecule hydrogen-bonded to Ala255 CO, Thr215 OH and the indole NH of Trp222. (e) Interior of the cytoplasmic half of the protein viewed from the extracellular side. (f) A cluster of hydrophobic residues from helix A', the BC loop and extracellular ends of helices A, B, F and G. O and N atoms are drawn in red and blue, respectively; C atoms are in pink (hydrophobic residues), yellow (acidic residues), slate (basic residues) or green (other residues).

cover a half part of the cytoplasmic surface of the protein.

Discussion

Structural comparison between pHr and shR

Unlike other archaeal rhodopsins, pHr possesses a short helix (A') in the N-terminal region. Another peculiar feature of pHr is a long inter-helical loop between helices B and C (Fig. 1). This loop is 10

residues longer than that of shR and covers a larger area of the extracellular surface (Fig. 6). Hydrophobic residues in the BC loop, together with those in helix A', form a hydrophobic cap at the extracellular surface of the protein. This hydrophobic cap helps us clarify the chloride uptake pathway, in which four residues (Arg123, Glu234, Arg176 and His100) and seven water molecules are aligned to form a long hydrogen-bonding network. The finding that His100 exists at the inlet of the chloride uptake pathway is consistent with the previous observation that the replacement of this histidine with alanine

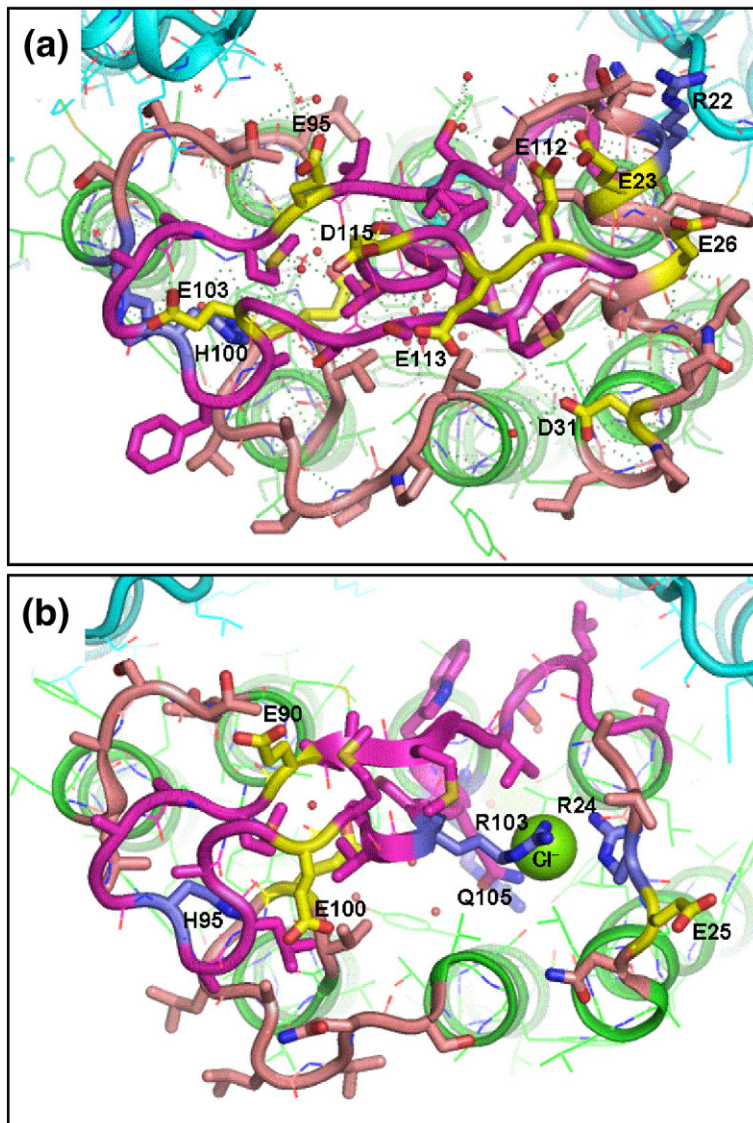


Fig. 6. (a, b) Extracellular loops in pH R (a) and sh R (b). O and N atoms are drawn in red and blue, respectively; C atoms are in yellow (acidic residues), slate (basic residues), magenta (hydrophobic residues in the BC loop), salmon (hydrophobic residues in helix A' and the DE and FG loops) or green (residues in transmembrane helices). The green sphere in (b) is a chloride ion bound to the secondary binding site of shR.

resulted in a significant decrease in chloride transport activity.³⁹ Because the deprotonation of Glu234 during the photocycle of pH R has been demonstrated,⁴⁰ it is likely that Glu234 functions as a gate in the chloride uptake pathway.

The hydrophobic cap mentioned above is absent in shR. Instead, shR possesses a secondary binding site of chloride that is surrounded by Arg24, Arg103 and Gln105.¹⁸ Whereas Arg24 is exposed to the external medium, Gln105 is connected to the primary binding site via a hydrogen-bonding network. Thus, the secondary anion binding site in shR is likely to constitute part of the chloride uptake pathway. It is noteworthy that an arginine residue (R103) that occurs at the extracellular end of helix C of shR is not found in pH R (Fig. 1). In fact, the corresponding place where shR possesses the secondary Cl^- binding site is occupied by the

extracellular hydrophobic cap in pH R. [Although pH R possesses the secondary binding site of chloride, it is located at the cytoplasmic surface (Fig. 4f).] This implies that there is a fundamental difference in the architecture of the chloride uptake pathway between shR and pH R. We propose that the extracellular hydrophobic cap in pH R plays a role in preventing a rapid exchange of chloride ion between the active site and the extracellular medium. This proposal is in harmony with previous observations that the decay of the O intermediate, which corresponds to the process of chloride uptake from the extracellular medium, is much slower in pH R than in shR.^{9,25,26} Actually, the O intermediate is undetectable in the *trans* photocycle of shR because its lifetime is very short.²⁶ It is conceivable that the longer lifetime of O in pH R than in shR contributes to the maintenance of the high activity of chloride pumping at high pH,

where the chloride release into the cytoplasmic medium can be slow.

The structure of the retinal-binding pocket is well conserved between pHr and shR (Fig. 7). All the residues contacting the retinal polyene chain are placed at identical positions in the structural models of pHr and shR. The distance between the Schiff base and the chloride ion in the primary binding site is also conserved. However, three water molecules (Wat502, Wat503 and Wat504) in the active centre are arranged differently in pHr and shR. The water distribution correlates with the conformation of a threonine in the middle of helix C (Thr126 in pHr/Thr111 in shR). Whereas Thr126 OH in pHr directs toward the chloride ion, Thr111 OH in shR is hydrogen-bonded to the carboxyl group of the fatty acid palmitate incorporated to the central open space of the trimer. This subtle difference seems to explain why the affinity of Cl^- to the primary binding site is much higher in pHr than in shR; that is, the dissociation constants of chloride for pHr and shR were reported to be ~ 1 and ~ 10 mM, respectively.^{21,23,24}

Quaternary structure of archaeal rhodopsins

It was previously shown that aR2 from *Halorubrum* sp. aus-2 forms a trimeric assembly in the presence of native lipids.³³ In Fig. 8a, the trimeric protein–bacterioruberin complex in the C2 crystal of

pHr is compared with that observed in the hexagonal P321 crystal of aR2. As long as the transmembrane region is discussed, the structural models of pHr and aR2 are very similar to each other. This similarity is astonishing when the sequence identity (28%) between pHr and aR2 is taken into account.³⁸

The binding site of bacterioruberin is also conserved in these proteins. In both cases, the cytoplasmic half of bacterioruberin is buried in a crevice between helices AB and DE of neighbouring protomers. From the similarity of the quaternary structure, one might argue that the same recognition mechanism of bacterioruberin is utilised by these proteins. However, most residues participating in the binding of bacterioruberin are not conserved between pHr and aR2. To understand the recognition mechanism of bacterioruberin, one needs to take into account many factors, including the morphology of the inter-subunit crevice. It should be mentioned that the trimeric structure of BR in the purple membrane of *H. salinarum* is also very similar to those shown in Fig. 8a.⁴¹ In the case of BR, a different lipid component (i.e., phospholipid) occupies the inter-subunit crevice, the morphology of which is not complementary to the shape of bacterioruberin.⁴² This example shows that bacterioruberin is not necessarily required for the oligomerisation of halobacterial rhodopsins. The question of why bacterioruberin binds to pHr or aR2 then arises. It has recently been shown that

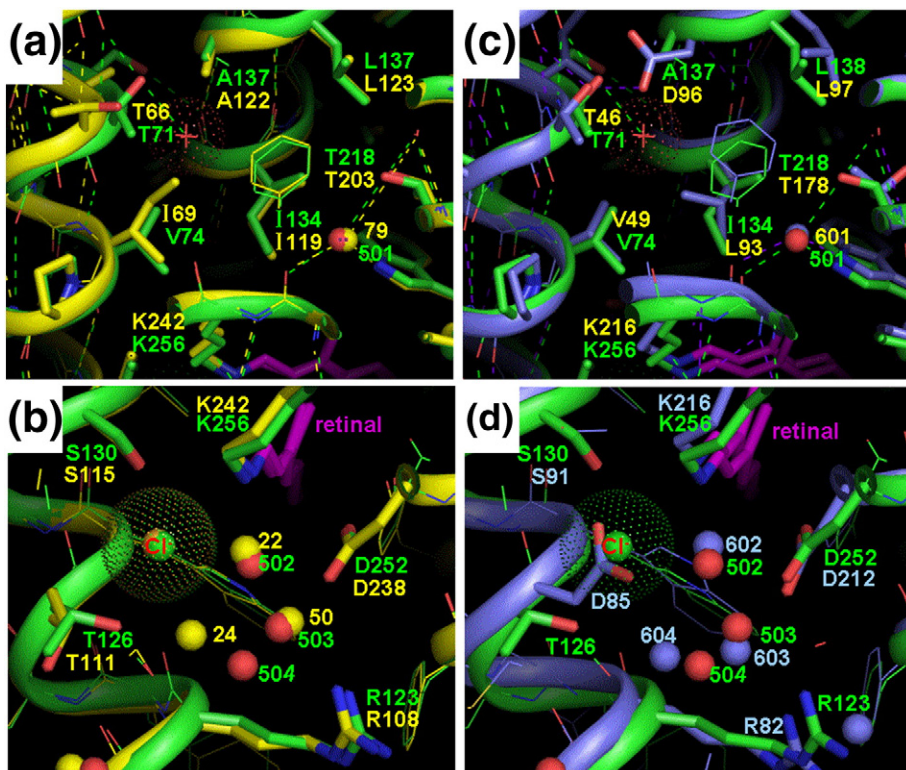


Fig. 7. Structural comparison between pHR and shR (left panels) and that between pHR and BR (right panels). (a, c) The cytoplasmic side of the retinal Schiff base. (b, d) The extracellular side of the retinal Schiff base. C atoms and water molecules in pHR, shR and BR are depicted in green, yellow and slate, respectively. Chloride ions in pHR and shR are in green and yellow dots, respectively.

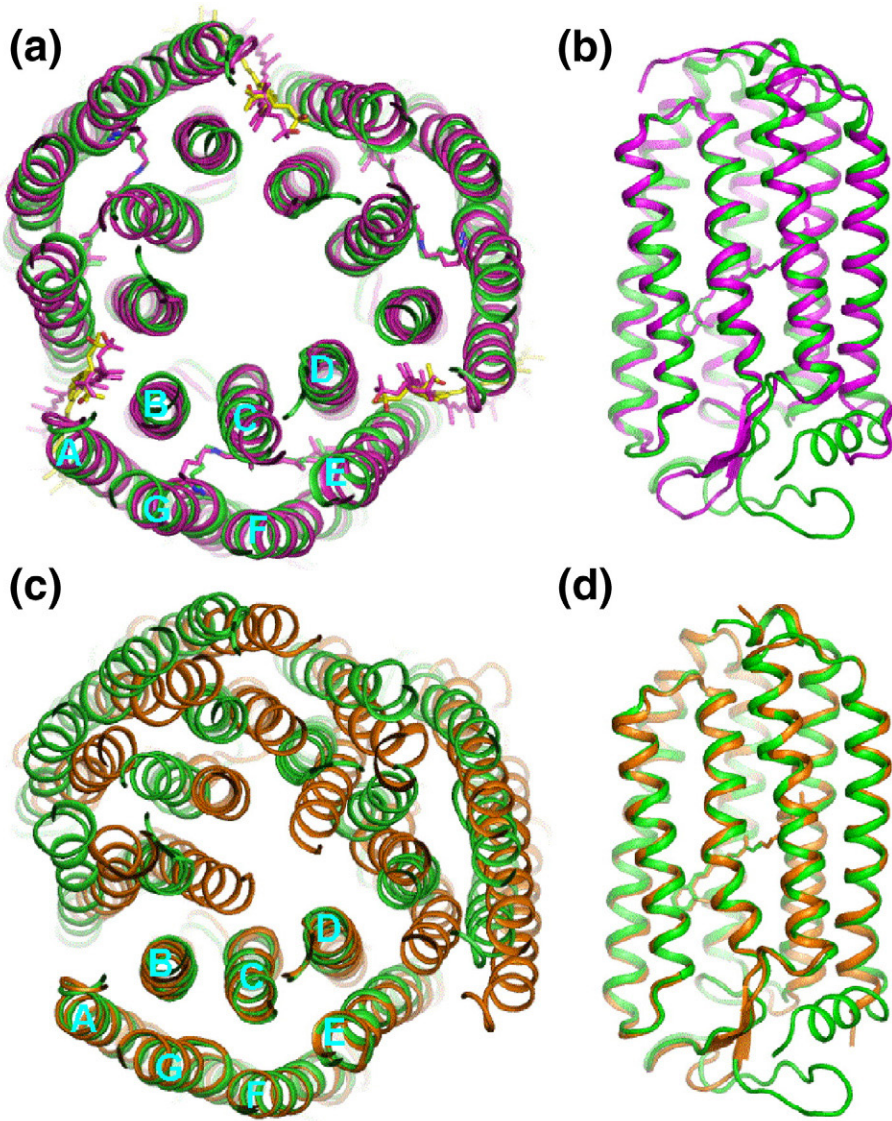


Fig. 8. (a, b) The trimeric and protomer structures of phR (green) are compared with those of aR2 (magenta). (c, d) The structures of phR (green) are compared with those of shR (orange).

xanthorhodopsin, a light-driven proton pump found in halophilic eubacteria, utilises salinixanthin as an antenna molecule for the efficient capture of solar energy.⁴³ In the trimeric structure of aR2 or phR, however, the geometric relationship between retinal and bacterioruberin is not optimised for the efficient energy transfer between these chromophores.³³ After all, the conceivable physiological roles of bacterioruberin in phR are to protect the protein against the harmful intensities of sunlight and/or to regulate pumping activity by sensing membrane potential. The second possibility is valuable for further consideration because the absorption spectrum of bacterioruberin bound to HR is sensitive to the membrane potential.⁴⁴

It was reported that shR formed a trimeric assembly in the hexagonal $P6_{3}22$ crystal that was prepared by the lipidic cubic phase method.¹⁸ However, the monomers in the shR trimer are tilted $\sim 11^\circ$ relative to the monomers in the phR or BR trimer (Fig. 8c). In other words, the shR protomers

are arranged in such a manner that no lipid is accommodated in the inter-subunit crevice. It is possible that the native quaternary structure of shR, which might be similar to those shown in Fig. 8a, is destroyed when native lipids are removed during the protein purification or crystallisation processes. In fact, the $P6_{3}22$ crystal of shR contained the fatty acid palmitate, which is not an endogenous lipid produced by *H. salinarum*.⁴⁵ Although the physiological role of palmitate is unknown, its existence near the Schiff base seems to affect the spectroscopic properties of a purified sample of shR.

Structural comparison between phR and BR

Despite different ions transported, the structure of the retinal-binding pocket is well conserved between phR and BR (or aR2). When the structural model of phR is superimposed on the BR model, the

chloride ion in *pHR* comes to the same position as that occupied by the carboxyl group of Asp85 in BR (Fig. 7d). Therefore, the charge distribution around the protonated Schiff base is eventually conserved between *pHR* and BR. The distribution of three water molecules (Wat502, Wat503 and Wat504) between the Schiff base and Arg123 (Arg82 in BR) is also conserved in these proteins. This coincidence suggests that the proper arrangement of water molecules in the active centre is necessary for efficient energy storage within the protein after light absorption, as proposed by other studies.⁴⁶

Similar to other archaeal rhodopsins, *pHR* possesses a proline residue (Pro132) that is responsible for a kink in the middle of helix C. Previous structural analyses of BR's reaction intermediates have shown that the extracellular part of helix C undergoes a large movement upon formation of the M state.^{37,47–49} Because key residues (Arg123, Tyr124 and Trp127) in this moiety are conserved in *pHR*, it

seems possible that during the ion pumping cycle of *pHR* the extracellular part of helix C undergoes the same conformational change as that observed during the proton pumping cycle of BR. It is noteworthy that the morphology of the central open space in the trimeric assembly is conserved between *pHR* and BR (or ar2). This suggests the possibility that their trimeric structure is designed to capture special lipid components that allow light-induced conformational changes in helix C.

The structural similarity between HR and BR is also seen in the cytoplasmic side of the retinal-binding pocket (Fig. 7c). Although Asp96 in BR is replaced by alanine in *pHR*, the micro-cavity between the main-chain carbonyl of Lys256 and the side chain of Thr71 (Thr46 in BR) is conserved (Fig. 9). Recent studies of the M→N transition of BR have suggested that the proton transfer from Asp96 to the deprotonated Schiff base takes place along a chain cluster of water molecules that is

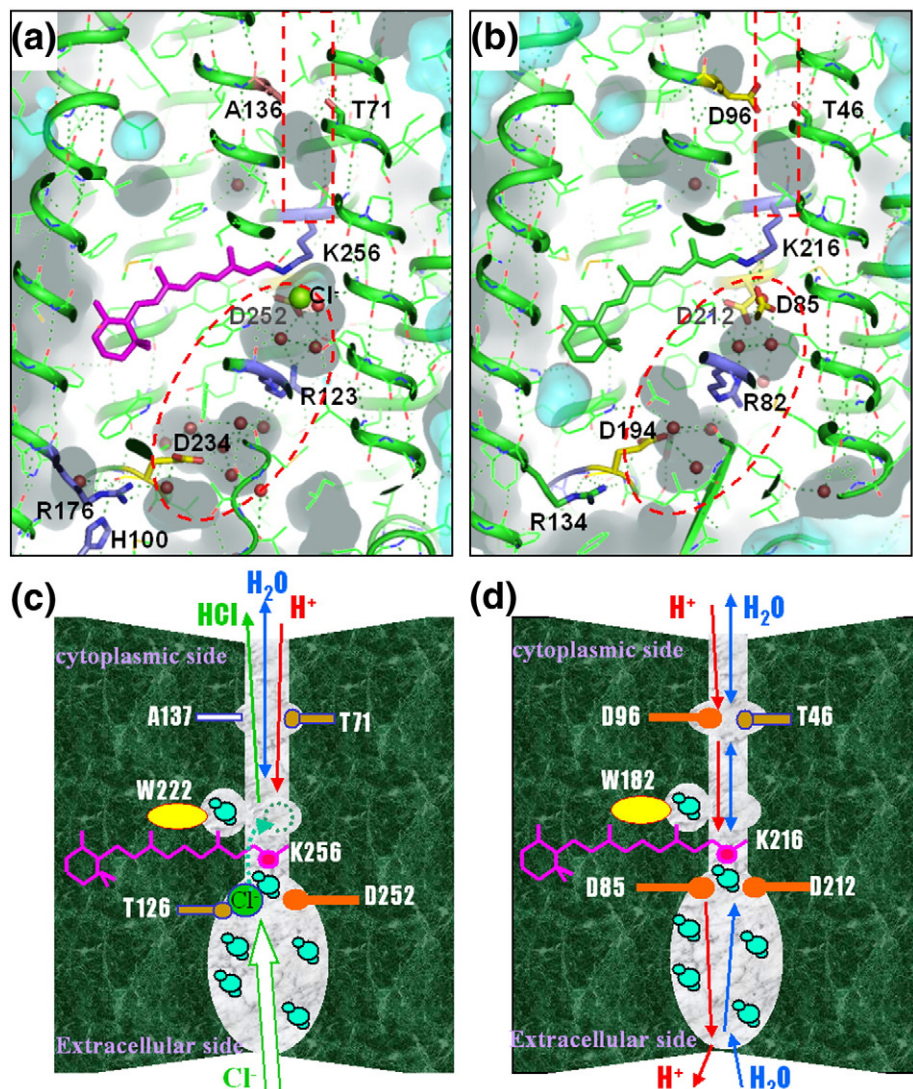


Fig. 9. (a, b) Micro-cavities in *pHR* (a) and BR (b) are drawn in cyan or grey. (c, d) Schematic representations of the mechanisms of Cl⁻ pumping in *pHR* (c) and proton pumping in BR (d). In this scheme, BR and HR are regarded as a proton/water antiporter and a proton/HCl antiporter, respectively.

transiently formed when the inter-helical cavity is widened.^{50–52} By contrast, it was reported that HR is converted to a light-driven proton pump when the chloride ion in the primary binding site is replaced by an inorganic base, azide.^{53–55} [There was controversial discussion about the effect of azide on the functionality of HR, which may be dependent on whether shR or phR is investigated. Our recent crystallographic study of the phR–azide complex showed that azide ion binds to a position between the Schiff base and Thr126 OH (our unpublished data), supporting the hypothetical scheme in which the bound azide functions as a proton acceptor of the Schiff base.⁵⁵] Thus, it is reasonable to suppose that the normal chloride pumping cycle of HR also involves a water-mediated proton transfer from the cytoplasmic surface to the anion, which is relocated to the cytoplasmic channel during the photocycle. It is worthwhile noting that inter-helical space in the cytoplasmic half of phR is filled mostly with hydrophobic residues. Although it was previously considered that Lys226 in helix F constitutes an anion release site, the structural data show that its side chain points outward to interact with the head groups of lipids. Because no ionisable residue exists in the inter-helical space of the cytoplasmic half, it can be argued that this moiety forms a large energetic barrier against the transport of a negatively charged ion. It seems natural to suppose that the height of this energetic barrier would be substantially lowered if the cytoplasmic half of HR functions as a proton/HCl antiporter, the net output of which is equivalent to the active transport of Cl[−] (Fig. 9c). This supposition would be in agreement with the notion that the chloride is transferred into the cytosol via diffusion.⁵⁶

It was reported that BR is converted into a light-driven chloride ion pump when a chloride binding site is created by the replacement of Asp85 with a threonine.⁵⁷ It was also suggested that the acid purple form of BR, in which a chloride binding site is created through the protonation of Asp85, pumps chloride ion under illumination.⁵⁸ These observations led several studies to propose an intriguing hypothesis that BR pumps hydroxyl ions, instead of protons. But, according to more recent structural data of photoreaction intermediates of BR,^{36,59} it is necessary to propose the hypothesis that BR functions as a proton/water antiporter, whereas HR functions as a proton/HCl antiporter. The structural data of phR suggest that this new hypothesis is valuable for further investigation.

Materials and Methods

Preparation of phR

The *N. pharaonis* strain KM-1, which was generated by UV mutagenesis from the type strain DSM 2160^T, was grown as described previously.¹⁶ The cells harvested were suspended in 3 M NaCl and 50 mM Hepes, pH 7.0; after

two cycles of freeze–thaw, the suspension was centrifuged at 10,000g for 15 min to remove unbroken cells, and the supernatant was centrifuged at 200,000g for 10 min at 4 °C to collect cell membranes. The cell membranes were washed three times with 100 mM NaCl and 50 mM Hepes, pH 7.0, and twice with distilled water.

Crystallisation of phR

For crystallisation of phR, the claret membrane was partially delipidated with 0.5% Tween-20 in 0.1 M NaCl, pH 7.0. Then, the crude claret membrane containing 2 mg/ml of phR was mixed with 5 mg/ml of nonylglucoside, 1.0 M ammonium sulfate, 0.16 M NaCl, 0.04% NaN₃ and 0.04 M Na citrate, pH 8.0. After 1 h of incubation at room temperature, the mixture was concentrated at 4000g for 10 min to remove other protein components, and the supernatant was collected. When a drop (~20 µl) of the supernatant was placed on a lower glass in the crystallisation plate and concentrated at 15 °C by the vapour diffusion method using 0.5 ml of 2.2–2.9 M ammonium sulfate and pH buffer as a reservoir solution, significant phase separation took place in a few days (i.e., phR molecules moved to a protein-rich phase floating in the solution or adhering to the lower glass). When the crystallisation solution was further incubated for ~4 weeks, crystals grew within the protein-rich phase. A typical crystal used for diffraction measured 0.7 mm × 0.05 mm × 0.05 mm.

Measurements of absorption spectra

Absorption spectra of a crystal of phR were measured using a microspectrophotometer, in which monochromatic light from a double monochromator (Shimadzu UV350A) was passed through a pinhole with a diameter of 0.1 mm and focused on a small area of the crystal. The transmitted light intensity was monitored with a photomultiplier tube.⁶⁰

Data collection and scaling

X-ray diffraction measurements were performed at beamlines SPring8-BL38B1 and SPring8-BL41XU, where a frozen crystal kept at 100 K was exposed to a monochromatic X-ray beam at a wavelength of 1.0 Å with an X-ray flux rate of ~2 × 10¹² photons/mm²/s. Diffraction data were collected using a CCD detector (Mar), with an oscillation range of 1° and an X-ray flux of 2 × 10¹³ photons/mm² per image. Indexing and integration of diffraction spots were carried out with Mosflm 6.1.⁶¹ The scaling of data was done using SCALA in the CCP4 program suites.⁶² Diffraction data from the phR crystal were fitted well by the cell dimensions of $a=151.83$ Å, $b=99.77$ Å, $c=99.27$ Å, $\alpha=90.0$, $\beta=127.67$ and $\gamma=90.0$. Crystal parameters and data collection statistics are summarised in Table 1.

Structural refinement

Model building was performed by the molecular replacement method using the previously reported model of HR (Protein Data Bank ID 1ed2) as an initial search model. Structure refinement was done using CNS 1.1⁶³ and XtalView 4.0.⁶⁴ After various trials, the space group was assigned to C2. Taking into account the size of

HR, it is suggested that one trimer of HR is packed in the asymmetric unit. Together with the result of linear dichroism, structural analysis suggested that the proteins are aligned in such a manner that the transmembrane helices orient nearly parallel with the *b*-axis. Although pH R is synthesised as a protein of 291 amino acids, the polypeptide chain from Val19 to Gly276 is traced in the current structural model of pH R.

Accession number

Crystallographic coordinates of pH R have been deposited in the Protein Data Bank with accession code 3A7K.

Acknowledgements

This work was supported by a grant from the Ministry of Education, Science and Culture of Japan. We thank Drs. N. Shimidzu and S. Baba for helping with the data collection at beamlines BL38B1 and BL41XU of SPring8.

References

- Mukohata, Y. & Kaji, Y. (1981). Light-induced ATP synthesis dependent on halorhodopsin-pH regulation. *Arch. Biochem. Biophys.* **208**, 615–617.
- Schobert, B. & Lanyi, J. K. (1982). Halorhodopsin is a light-driven chloride pump. *J. Biol. Chem.* **257**, 10306–10313.
- Bivin, D. B. & Stoeckenius, W. (1986). Photoactive retinal pigments in haloalkaliphilic bacteria. *J. Gen. Microbiol.* **132**, 2167–2177.
- Váró, G. (2000). Analogies between halorhodopsin and bacteriorhodopsin. *Biochim. Biophys. Acta*, **1460**, 220–229.
- Essen, L.-O. (2002). Halorhodopsin: light-driven ion pumping made simple? *Curr. Opin. Struct. Biol.* **12**, 516–522.
- Cisneros, D., Oesterhelt, D. & Müller, D. J. (2005). Probing origins of molecular interactions stabilizing the membrane proteins halorhodopsin and bacteriorhodopsin. *Structure*, **13**, 235–242.
- Peters, F., Herbst, J., Tittor, J., Oesterhelt, D. & Dillerd, R. (2006). Primary reaction dynamics of halorhodopsin, observed by sub-picosecond IR-vibrational spectroscopy. *Chem. Phys.* **323**, 109–116.
- Gruia, A. D., Bondar, A. N., Smith, J. C. & Fischer, S. (2006). Mechanism of a molecular valve in the halorhodopsin chloride pump. *Structure*, **13**, 617–627.
- Guijarro, J., Engelhard, M. & Siebert, F. (2006). Anion uptake in halorhodopsin from *Natronomonas pharaonis* studied by FTIR spectroscopy: consequences for the anion transport mechanism. *Biochemistry*, **45**, 11578–11588.
- Magyari, K., Simon, V. & Váró, G. (2006). The influence of the halide ions on the photochemical reaction cycle of *pharaonis* halorhodopsin. *J. Photochem. Photobiol. B*, **82**, 16–20.
- Inoue, K., Kubo, M., Demura, M., Kamo, N. & Terazima, M. (2006). Reaction dynamics of halorhodopsin studied by time-resolved diffusion. *Biophys. J.* **96**, 3724–3734.
- Seki, A., Miyauchi, S., Hayashi, S., Kikukawa, T., Kubo, M., Demura, M. et al. (2007). Heterologous expression of *pharaonis* halorhodopsin in *Xenopus laevis* oocytes and electrophysiological characterization of its light-driven Cl[−] pump activity. *Biophys. J.* **92**, 2559–2569.
- Gradinaru, V., Thompson, K. R. & Deisseroth, K. (2008). eNpHR: a *Natronomonas* halorhodopsin enhanced for optogenetic applications. *Brain Cell Biol.* **36**, 129–139.
- Nakamura, T., Takeuchi, S., Shibata, M., Demura, M., Kandori, H. & Tahara, T. (2008). Ultrafast pump-probe study of the primary photoreaction process in *pharaonis* halorhodopsin: halide ion dependence and isomerization dynamics. *J. Phys. Chem. B*, **112**, 12795–12800.
- Oesterhelt, D. (1995). Structure and function of halorhodopsin. *Isr. J. Chem.* **35**, 475–494.
- Ihara, K., Narusawa, A., Maruyama, K., Takeguchi, M. & Kouyama, T. (2008). A halorhodopsin-overproducing mutant isolated from an extremely haloalkaliphilic archaeon *Natronomonas pharaonis*. *FEBS Lett.* **582**, 2931–2936.
- Avetisyan, A. V., Kaulen, A. D., Skulachev, V. P. & Feniouk, B.A. (1998). Photophosphorylation in haloalkaliphilic halobacterial cells containing halorhodopsin: chloride-ion cycle? *Biochemistry (Moscow)*, **63**, 625–628.
- Falb, M., Pfeiffer, F., Palm, P., Rodewald, K., Hickmann, V., Tittor, J. & Oesterhelt, D. (2005). Living with two extremes: conclusions from the genome sequence of *Natronomonas pharaonis*. *Genome Res.* **15**, 1336–1343.
- Blanck, A. & Oesterhelt, D. (1987). The halo-opsin gene: II. Sequence, primary structure of halorhodopsin and comparison with bacteriorhodopsin. *EMBO J.* **6**, 265–273.
- Lanyi, J. K., Duschl, A., Hatfield, G. W., May, K. & Oesterhelt, D. (1990). The primary structure of a halorhodopsin from *Natronobacterium pharaonis*. Structural, functional and evolutionary implications for bacterial rhodopsins and halorhodopsins. *J. Biol. Chem.* **265**, 1253–1260.
- Scharf, B. & Engelhard, M. (1994). Blue halorhodopsin from *Natronobacterium pharaonis*: wavelength regulation by anions. *Biochemistry*, **33**, 6387–6393.
- Ogurusu, T., Maeda, A., Sasaki, N. & Yoshizawa, T. (1981). Light-induced reaction of halorhodopsin prepared under low salt conditions. *J. Biochem. (Tokyo)*, **90**, 1267–1273.
- Duschl, A., Lanyi, J. K. & Zimányi, L. (1990). Properties and photochemistry of a halorhodopsin from the haloalkaliphile, *Natronobacterium pharaonis*. *J. Biol. Chem.* **265**, 1261–1267.
- Schobert, B., Lanyi, J. K. & Oesterhelt, D. (1986). Effects of anion binding on the deprotonation reactions of halorhodopsin. *J. Biol. Chem.* **261**, 2690–2696.
- Hackmann, C., Guijarro, J., Chizhov, I., Engelhard, M., Rödig, M. & Siebert, F. (2001). Static and time-resolved step-scan Fourier transform infrared investigations of the photoreaction of halorhodopsin from *Natronobacterium pharaonis*: consequences for models of the anion translocation mechanism. *Biophys. J.* **81**, 394–406.
- Varo, G., Zimanyi, L., Fan, X., Sun, X., Needleman, R. & Lanyi, J. K. (1995). Photocycle of halorhodopsin from *Halobacterium salinarium*. *Biophys. J.* **68**, 2062–2072.
- Kunji, E. R. S., von Gronau, S., Oesterhelt, D. & Henderson, R. (2000). The three-dimensional structure of halorhodopsin to 5 Å by electron crystallography: a new unbending procedure for two-dimensional

- crystals by using a global reference structure. *Proc. Natl Acad. Sci. USA*, **97**, 4637–4642.
28. Kolbe, M., Besir, H., Essen, L. R. & Oesterhelt, D. (2000). Structure of the light-driven chloride pump halorhodopsin at 1.8 Å resolution. *Science*, **288**, 1390–1396.
 29. Gmelin, W., Zeth, K., Efremov, R., Heberle, J., Tittor, J. & Oesterhelt, D. (2007). The crystal structure of the L1 intermediate of halorhodopsin at 1.9 Å resolution. *Photochem. Photobiol.* **83**, 369–377.
 30. Rüdiger, M. & Oesterhelt, D. (1997). Specific arginine and threonine residues control anion binding and transport in the light-driven chloride pump halorhodopsin. *EMBO J.* **16**, 3813–3821.
 31. Zimányi, L. & Lanyi, J. K. (1997). Fourier transform Raman study of retinal isomeric composition and equilibration in halorhodopsin. *J. Phys. Chem. B*, **101**, 1930–1933.
 32. Gerscher, S., Mylrajan, M., Hildebrandt, P., Baron, M. H., Müller, R. & Engelhard, M. (1997). Chromophore–anion interactions in halorhodopsin from *Natronobacterium pharaonis* probed by time-resolved resonance Raman spectroscopy. *Biochemistry*, **36**, 11012–11020.
 33. Yoshimura, K. & Kouyama, T. (2008). Structural role of bacterioruberin in the trimeric structure of archaeorhodopsin-2. *J. Mol. Biol.* **375**, 1267–1281.
 34. Takeda, K., Sato, H., Hino, T., Kono, M., Fukuda, K., Sakurai, I. et al. (1998). A novel three-dimensional crystal of bacteriorhodopsin obtained by successive fusion of the vesicular assemblies. *J. Mol. Biol.* **283**, 463–474.
 35. DeLano Scientific (2006). PyMOL version 0.99. <http://pymol.sourceforge.net>.
 36. Yamamoto, M., Hayakawa, N., Murakami, M. & Kouyama, T. (2009). Crystal structures of different sub-states of bacteriorhodopsin's M intermediate at various pH levels. *J. Mol. Biol.* **393**, 559–573.
 37. Sasaki, T., Kubo, M., Kikukawa, T., Kamiya, M., Aizawa, T., Kawano, K. & Kamo, N. (2008). Halorhodopsin from *Natronomonas pharaonis* forms a trimer even in the presence of a detergent, dodecyl-beta-D-maltoside. *Photochem. Photobiol.* **85**, 130–136.
 38. Mukohata, Y., Ihara, K., Tamura, T. & Sugiyama, Y. (1999). Halobacterial rhodopsins. *J. Biochem.* **125**, 649–657.
 39. Otomo, J. (1995). Anion selectivity and pumping mechanism of halorhodopsin. *Biophys. Chem.* **56**, 137–141.
 40. Shibata, M., Saito, Y., Demura, M. & Kandori, H. (2006). Deprotonation of Glu234 during the photocycle of *Natronomonas pharaonis* halorhodopsin. *Chem. Phys. Lett.* **432**, 545–547.
 41. Grigorieff, N., Ceska, T. A., Downing, K. H., Baldwin, J. M. & Henderson, R. (1996). Electron-crystallographic refinement of the structure of bacteriorhodopsin. *J. Mol. Biol.* **259**, 393–421.
 42. Sato, H., Takeda, K., Tani, K., Hino, T., Okada, T., Kouyama, T. et al. (1999). Specific lipid–protein interactions in a novel honeycomb lattice structure of bacteriorhodopsin. *Acta Crystallogr., Sect. D: Biol. Crystallogr.* **55**, 1251–1256.
 43. Balashov, S. P., Imasheva, E. S., Boichenko, V. A., Antón, J., Wang, J. M. & Lanyi, J. K. (2005). Xanthorhodopsin: a proton pump with a light-harvesting carotenoid antenna. *Science*, **309**, 2061–2064.
 44. Seki, S., Sasabe, H. & Tomioka, H. (1996). Voltage-dependent absorbance change of carotenoids in halophilic archaeabacteria. *Biochim. Biophys. Acta*, **1284**, 79–85.
 45. Corcelli, A., Lobasso, S., Colella, M., Trotta, M., Guerrieri, A. & Palmisano, A. (1996). Role of palmitic acid on the isolation and properties of halorhodopsin. *Biochim. Biophys. Acta*, **1281**, 173–181.
 46. Shibata, M., Muneda, N., Sasaki, T., Shimono, K., Kamo, N., Demura, M. & Kandori, H. (2005). Hydrogen-bonding alterations of the protonated Schiff base and water molecule in the chloride pump of *Natronobacterium pharaonis*. *Biochemistry*, **44**, 12279–12286.
 47. Luecke, H., Schobert, B., Richter, H.-T., Cartailler, J.-P. & Lanyi, J. K. (1999). Structural changes in bacteriorhodopsin during ion transport at 2 angstrom resolution. *Science*, **286**, 255–260.
 48. Facciotti, M. T., Rouhani, S., Burkard, F. T., Betancourt, F. M., Downing, K. H., Rose, R. B. et al. (2001). Structure of an early intermediate in the M-state phase of the bacteriorhodopsin photocycle. *Biophys. J.* **81**, 3442–3455.
 49. Takeda, K., Matsui, Y., Kamiya, N., Adachi, S., Okumura, H. & Kouyama, T. (2004). Crystal structure of the M intermediate of bacteriorhodopsin: allosteric structural changes mediated by sliding movement of a transmembrane helix. *J. Mol. Biol.* **341**, 1023–1037.
 50. Cao, Y., Váró, G., Chang, M., Ni, B., Needleman, R. & Lanyi, J. K. (1991). Water is required for proton transfer from aspartate-96 to the bacteriorhodopsin Schiff base. *Biochemistry*, **30**, 10972–10979.
 51. Maeda, A., Morgan, J. E., Gennis, R. B. & Ebrey, T. G. (2006). Water as a cofactor in the unidirectional light-driven proton transfer steps in bacteriorhodopsin. *Photochem. Photobiol.* **82**, 1398–1405.
 52. Hayakawa, N., Kasahara, T., Hasegawa, D., Yoshimura, K., Murakami, M. & Kouyama, T. (2008). Effect of xenon binding to a hydrophobic cavity on the proton pumping cycle in bacteriorhodopsin. *J. Mol. Biol.* **384**, 812–823.
 53. Hegemann, P., Oesterhelt, D. & Steiner, M. (1985). The photocycle of the chloride pump halorhodopsin: I. Azide-catalyzed deprotonation of the chromophore is a side reaction of photocycle intermediates inactivating the pump. *EMBO J.* **4**, 2347–2350.
 54. Bamberg, E., Tittor, J. & Oesterhelt, D. (1993). Light-driven proton or chloride pumping by halorhodopsin. *Proc. Natl Acad. Sci. USA*, **90**, 639–643.
 55. Váró, G., Brown, L. S., Needleman, R. & Lanyi, J. K. (1996). Proton transport by halorhodopsin. *Biochemistry*, **35**, 6604–6611.
 56. Sato, M., Kubo, M., Aizawa, T., Kamo, N., Kikukawa, T., Nitta, K. & Demura, M. (2005). Role of putative anion-binding sites in cytoplasmic and extracellular channels of *Natronomonas pharaonis* halorhodopsin. *Biochemistry*, **44**, 4775–4784.
 57. Sasaki, J., Brown, L. S., Chon, Y. S., Kandori, H., Maeda, A., Needleman, R. & Lanyi, J. K. (1995). Conversion of bacteriorhodopsin into a chloride ion pump. *Science*, **269**, 73–75.
 58. Dér, A., Szaraz, S., Tóth-Boconadi, R., Tokaji, Z., Keszthelyi, L. & Stoeckenius, W. (1991). Alternative translocation of protons and halide ions by bacteriorhodopsin. *Proc. Natl Acad. Sci. USA*, **88**, 4751–4755.
 59. Kouyama, T., Nishikawa, T., Tokuhisa, T. & Okumura, H. (2003). Crystal structure of the L intermediate of bacteriorhodopsin: evidence for vertical translocation of a water molecule during the proton pumping cycle. *J. Mol. Biol.* **335**, 531–546.
 60. Sakai, K., Matsui, Y., Kouyama, T., Shiro, Y. & Adachi, S. (2002). Optical monitoring of freeze-trapped reaction intermediates in protein crystals: a microspectrophotometer for cryogenic protein crystallography. *J. Appl. Crystallogr.* **35**, 270–273.

61. Steller, I., Bolotovsky, B. & Rossmann, M. G. (1997). An algorithm for automatic indexing of oscillation images using Fourier analysis. *J. Appl. Crystallogr.* **30**, 1036–1040.
62. Collaborative Computational Project, Number 4. (1994). The CCP4 suite: programs for protein crystallography. *Acta Crystallogr., Sect. D: Biol. Crystallogr.* **50**, 760–763.
63. Brünger, A. T., Adams, P. D., Glore, G. M., Delano, W. L., Gros, P., Grosse-Kunstleve, R. W. *et al.* (1998). Crystallography & NMR System (CNS): a new software system for macromolecular structure determination. *Acta Crystallogr., Sect. D: Biol. Crystallogr.* **54**, 905–921.
64. McRee, D. E. (1993). *Practical Protein Crystallography*. Academic Press, San Diego, CA.